

# Measurements of the laminar burning velocity for mixtures of methanol and air from a constant-volume vessel using a multizone model

Khizer Saeed<sup>a</sup>, C.R. Stone<sup>b,\*</sup>

<sup>a</sup> Department of Mechanical Engineering, Aligarh M University, Aligarh 202002, India

<sup>b</sup> Department of Engineering Sciences, Oxford University, Parks Road, Oxford OX1 3PJ, UK

Received 17 December 2003; received in revised form 6 August 2004; accepted 10 August 2004

Available online 11 September 2004

## Abstract

A novel multiple burned gas zone model has been used to determine the temperature distribution within the burned gas and the relationship between the pressure rise and the mass fraction burned in a constant-volume vessel. This computation allows for the variation in heat capacity of the constituents and solves the equilibrium combustion equation for the 10 major species: N<sub>2</sub>, O<sub>2</sub>, H<sub>2</sub>, CO, CO<sub>2</sub>, H<sub>2</sub>O, O, H, NO, and OH. A constant-volume spherical vessel has been used for measuring burning rates for liquid fuels at elevated initial temperatures and pressures. A heating system and a mixing system were installed for measurements at elevated initial temperatures and for preparing mixtures of liquid fuels. The test facility has been used for generating reproducible data for both gaseous and liquid fuels. Using the multizone model, the laminar burning velocity has been found for mixtures of methanol–air with initial temperatures of 293.15 and 425 K, initial pressures of 0.5, 1.0, 2.0, and 3.5 bar, and equivalence ratios of 0.8 to 1.6. The laminar burning velocities were fitted to a seven-term equation to describe the effects of stoichiometry, pressure, and temperature. The burning velocities for methanol–air have been compared with earlier measurements; the values obtained from the present study give very good agreement with the recently reported data of Davis and Law for ambient pressure and temperature. Cellular flames were found to exist in some test runs and the conditions of its onset are reported.

© 2004 The Combustion Institute. Published by Elsevier Inc. All rights reserved.

## 1. Introduction

One of the distinguishing features of laminar pre-mixed flames is that they have a characteristic propagation rate, commonly called the burning velocity. The burning velocity,  $S_u$ , is more precisely defined as

the velocity at which unburned gases move through the combustion wave in the direction normal to the wave surface. Laminar burning velocities are of great significance, since they are used in many areas of combustion science such as in designing burners and predicting explosions. They play essential roles in determining several important aspects of the combustion process in spark ignition engines; among these are the ignition delay (which in turn affects the range of equivalence ratios over which an engine can be operated and cycle to cycle variations), the thickness of

\* Corresponding author.

E-mail address: [richard.stone@eng.ox.ac.uk](mailto:richard.stone@eng.ox.ac.uk)  
(C.R. Stone).

the wall quench layers (which are a primary source of unburned hydrocarbons), and the minimum ignition energy. It is found that a detailed knowledge of laminar premixed flames will provide insights into such properties as heat release rates, flammability limits, propagation rates, quenching, and emissions characteristics. Flame chemistry is commonly studied by performing computer simulations of laminar one-dimensional flames by solving complex chemical kinetic schemes. But the chemical kinetic data in such models are not always sufficiently well known for the predictions to be used with confidence. It is common to use measured burning velocities to validate these chemical kinetic schemes. The production of accurate measurements on laminar premixed flames therefore plays a key role in the process of understanding a large range of flames. Although the majority of fuel is probably burnt in turbulent combustion, data on laminar burning velocities are still needed as inputs to many turbulent combustion models. Also, in internal combustion engines the initial combustion is laminar, so again there is a need for the laminar burning velocity.

There are several competing methods for determining a laminar burning velocity. These methods are divided into two classes: stationary and nonstationary flame methods. The two methods discussed next (the counterflow-burner method and the constant-volume method) are considered to be the most prominent.

The counterflow-burner technique is principally associated with Law's group, who have studied a very wide range of fuels. The method is convenient for both liquid and gaseous fuels, with good control of mixture composition. This technique is best suited to pressures and temperatures close to ambient, and it is necessary to correct for the effects on the burning velocity of strain in the complex flow fields; this correction procedure is still the subject of debate.

The constant-volume bomb method uses a spherical vessel with central ignition and relies on measurements taken after the early stages of flame propagation, during which there is a significant pressure rise. The advantage of measuring the burning velocity using the closed vessel over other methods is that, from a single test, burning velocities can be calculated over a wide range of temperatures and pressures. However, two conditions must be fulfilled for the correct determination of the burning velocities from this method. First, the pressure rise in the vessel due to combustion must be recorded correctly and, secondly, the equation used for determining burning velocities should be valid throughout the range of the pressure rise. Most burning velocity equations for a closed vessel have been found to be valid only in the initial stages of combustion (generally taken as  $\leq 1.1 P_i$ ). Of

all the models used, that of Lewis and von Elbe [1] is the simplest and that of Metghalchi and Keck [2] is the most comprehensive with separate burned and unburned zones. However, Stone et al. [3] have reported little variation between the two methods if the theoretical peak pressure is calculated from the STANJAN [4] package. A refinement of Metghalchi and Keck's two-zone approach has recently been presented [5], in which a thermal boundary layer has been added. The details of its implementation are not presented, nor are there any comparisons of results analyzed with and without heat transfer, so as to give an indication as to how significant heat transfer is.

Previous work [6] has shown that heat transfer to the walls is negligible, apart from the very final stages of combustion, which accounts for the lower than expected final pressure. This is detectable from the rate of pressure rise no longer increasing with time, leading to the rounding of the pressure record at maximum pressure and a change in the slope of the burning velocity when plotted against time; such data were not used.

The combustion inside a spherical closed vessel has been modeled here with a multizone model so as to gain more insight into the combustion process. The modeling has been with both an equal radial (EQR) distribution of zones and an equal mass (EQM) distribution of mass between the zones in the spherical vessel. Hopkinson [7] established that there is a temperature gradient in the burnt gas, and this difference can typically be 500 K at the end of combustion between the first and the last burned gas. O'Donnovan and Rallis [8] proposed its incorporation into the equation for calculating the burning velocity in a closed vessel. However, contradictory results have been found when the temperature gradient is modeled [9–12]. Results of modeling also show the nonlinear dependence of pressure on mass fraction burned. This leads to errors in the calculation of the burning velocities using Lewis and von Elbe's [1] method.

The laminar burning velocity is a function of not only the fuel/oxidant ratio but also the temperature and pressure of the system and the presence of any diluents in the mixture. The main aim of this work was to generate accurate experimental laminar burning velocities for widely varying conditions. Recent tests in a spark ignition engine have shown some surprising differences in the burn rates of liquid fuels, with the early burn period (0–10% mass fraction burn) of methanol being about half that of iso-octane [13]. Of these liquid fuels, there is a shortage of laminar burning velocity data for methanol at elevated temperatures and pressures.

## 2. Modeling

Computational studies, which have modeled combustion inside a closed constant-volume vessel, are those by Bradley and Mitcheson [9] and Takeno and Iijima [14]. However, both aimed to predict the rate of pressure rise, as opposed to using the models for deducing the burning velocity from experimental pressure records. The assumptions and a mathematical derivation of the time-dependent first order ordinary differential equations for the pressure and burned and unburned gas temperatures are presented here for the single-burned-gas-zone model, and the detailed derivation is discussed in Saeed [15]; the final equations for the multizone analysis are also in Appendix A. The single-burned-zone model was extended to two burned zones and then to multiple zones. To solve these equations, a BOMB program was developed by the Oxford Engine Group. The mass in the spherical vessel can be divided into the multiple zones in a number of ways. The two ways used here are equal mass zones (hereafter called the equal mass (EQM) model) or equal radial zones (hereafter called the equal radii (EQR) model); see Fig. 1.

In the multizone model, flame propagation is seen as the consecutive consumption of unburned mixture within the zones. Before ignition, the mass in the spherical vessel is divided into  $n$  zones. At the time when combustion has just begun in the bomb, the flame front will consume zone 1 first. As a result, the temperature and hence pressure of zone 1 will increase, thereby compressing the rest of the unburned gas (considered as single entity) and increasing the pressure inside the vessel to a higher value. After the consumption of the first zone, combustion of the second and subsequent zones will take place at a higher

pressure than the initial pressure. At any instant of time when the flame front is passing through the  $n$ th zone, the combustion of this zone takes place at a temperature of  $T_{u,n-1}$  ( $> T_i$ ) and a constant pressure  $P_{u,n-1}$  ( $> P_i$ ). The combustion within a given zone takes place progressively. After the flame has consumed the  $n$ th zone, it is then assumed to be adiabatic. Subsequent combustion further compresses the burned gas and the unburned gas. As a result, temperature and density gradients are established in the burned gas region. In the BOMB program, since the burnt gas in each zone will be at a different temperature, they each have a different composition. At each temperature the composition of the burnt gases is solved for equilibrium among the following species: CO, CO<sub>2</sub>, H<sub>2</sub>O, H<sub>2</sub>, H, OH, O, N<sub>2</sub>, NO, and O<sub>2</sub>. These equilibrium calculations are solved by minimizing the Gibbs energy, using a routine written by Ferguson [16]. The gases are assumed to behave as semiperfect gases, and the internal energy, entropy, and specific heat capacities are calculated from the polynomial functions for the specific heat capacity at different temperatures. As the specific heat capacity has a “knee” between 900 and 2000 K, a single polynomial is never likely to be satisfactory. Instead, two polynomials can be used; they give identical values of the specific heat, at the transition between the low range and the high range. The data used here are from Gordon and McBride [17], who used a transition temperature of 1000 K.

## 3. Model results

The BOMB program was run to model flame propagation inside the spherical combustion vessel; mixtures of methane–air have been considered for comparison with other work. A parametric study of the

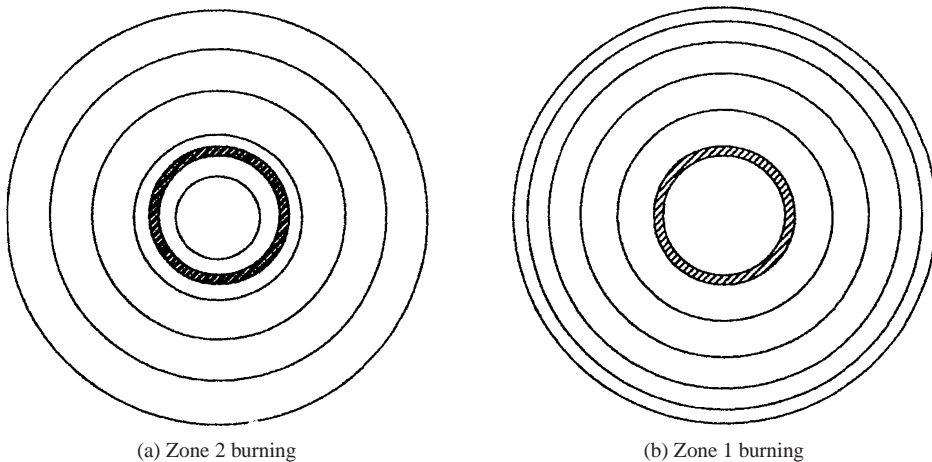


Fig. 1. Radial distribution of the multiple zones inside a spherical vessel. (a) Five zones equal mass model (EQM); (b) five zones equal radius model (EQR). Hatched portion indicates the position of the flame front at an instant of time.

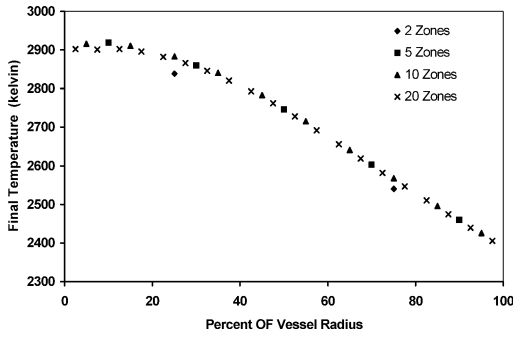


Fig. 2. Final variation of temperature with the zones in the equal radius (EQR) model with initial conditions of 1 bar and 298.15 K, for a stoichiometric methane–air mixture.

final radial temperature distribution across the vessel at the end of combustion, for different numbers of zones and numbers of steps in each zone, was made. The influence of the burned gas temperature gradient on pressure, errors in the mass fraction, and burning velocity at the initial elevated temperature and pressure and the effects of equivalence ratio on pressure and temperature were studied.

When combustion ends in a spherical vessel, the radial temperature distributions for the EQR model are as shown in Fig. 2. This shows that with an increase in the number of zones, the shape of the temperature profile becomes the same. As expected, a large number of zones will give the most accurate prediction. However, only very slight differences were found in the burned temperature distribution profile when the number of zones was increased from 20 to 50 and the number of steps was increased from 200 to 1000. Therefore, a finite number of zones can give a sufficiently accurate analysis of the phenomenon. Also, with a large number of zones, mass diffusion and heat transfer between the zones might need to be considered. To obtain sufficiently accurate results and to reduce the run time of the simulation, it was decided to use 10 zones and 200 steps for all the investigations reported here.

In Fig. 2, a comparison of a 20-zone model with a 2-zone model for the final temperature distribution shows a difference of nearly 90 K in the first burned zones and a difference of 110 K in the last burned zones. The end pressure obtained in the present study for methane/air mixtures is about 1.5% lower than that obtained by Bradley and Mitcheson [9] or Takeno and Iijima [14]; see Table 1. This could be due to the errors associated with the approximations that they made for the heat capacities of the gases. However, the EQM zone and EQR zone models have been validated here with the temperatures predicted by STANJAN [4].

Table 1

Comparison of the end pressure for stoichiometric methane–air combustion with initial conditions of 300 K and 1 bar

	Bradley and Mitcheson [9]	Takeno and Iijima [14]	Present study
End pressure (bar)	8.90	8.88	8.76

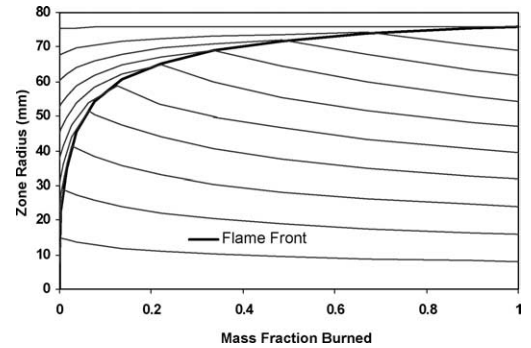


Fig. 3. Particle path across the spherical vessel for the 10-zone equal radii model (EQR) for a stoichiometric methane–air mixture, with initial conditions of 1 bar and 298.15 K.

Fig. 3 gives a greater physical insight into combustion inside the bomb, showing how the radius of each zone varies during the propagation of the flame front. As the flame front travels through the combustion bomb, each zone burns in succession. It can be seen from Fig. 3 that as the flame front travels through each zone an increase in the radius of that zone takes place. This is due to the expansion of the products of combustion immediately behind the flame front. When the flame front has passed the zone (which is indicated by the maximum radius of a particular zone), recompression of the zones takes place due to the expansion of the next zone. Due to the recompression, a decrease in the radii and hence the volume of the burned zones takes place. This results in an increase in the temperature of the burned gas zones, which establishes the radial burned gas temperature gradient. As the first burned zone is hotter than the outer zones it can be seen that Zone 1 finishes with a larger radius.

Fig. 4 shows the variation of the pressure with the mass fraction burned. A comparison of this variation with that of the linear Lewis and von Elbe [1] expression is also shown. It can be seen from the figure that the pressure variation with the mass fraction obtained in this study is nonlinear. Takeno and Iijima [14] also had a linear variation of the mass fraction burned to the pressure rise. However, from the present study it can be seen that throughout the process there is an overestimation of the pressure if a linear relationship is used, and the error is worst during the central part of combustion. Fig. 5 shows the percentage of error in

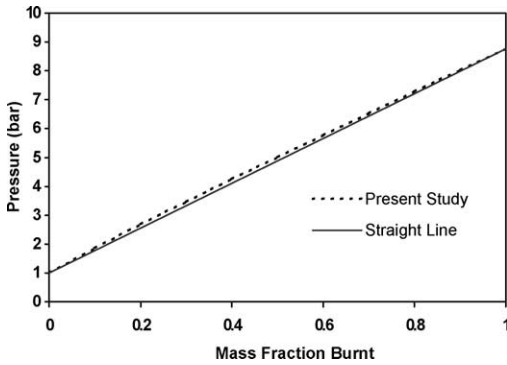


Fig. 4. Variation of the pressure with the mass fraction burnt for the 10-zone equal mass model (EQM) for stoichiometric methane–air mixture, with initial conditions of 1 bar and 298.15 K.

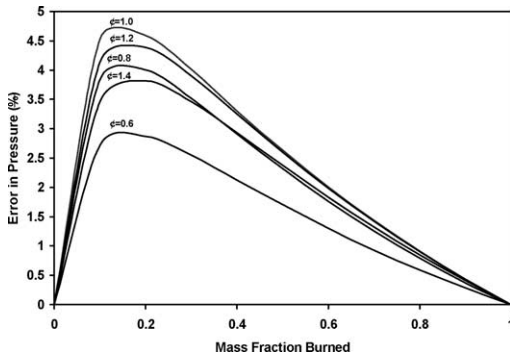


Fig. 5. Variations in pressure errors with mass fraction burnt for the 10-zone equal mass (EQM) model for initial conditions of 1 bar, 298.15 K, for stoichiometric methane–air mixtures.

pressure with the varying mass fraction burnt. It can be seen that the maximum error is for stoichiometric combustion. In Fig. 2, it was seen that a burned gas temperature gradient exists in a spherical vessel, a fact established by Hopkinson [7] in 1906. In the present analysis, a temperature difference of more than 450 K is found at the end of combustion for a stoichiometric methane–air mixture. Also, a considerable temperature difference between the predictions made by a single-zone model and those made by multiple-zone models is found.

#### 4. Experimental apparatus

Fig. 6 shows the apparatus used. It consists of the following: combustion vessel and heating system, ignition circuit, gaseous and liquid fuel handling system, and data acquisition system. The spherical test vessel (160 mm diameter) is provided with central ig-

nition electrodes and it can withstand a pressure of 34 bar. The combustion vessel is placed inside an oven, made from Sindanyo; it is fitted with a fan, temperature controller, and air baffle plate. The heating system is employed to achieve two purposes: testing of the mixture at elevated initial temperatures and vaporization of liquid fuels at high pressures. An initial temperature of 150 °C inside the test vessel can be achieved and maintained using the heating system. Ignition is by a standard Lucas inductive ignition system consisting of coil drive module, two extended equal-length electrodes, a 12-V battery, and a switching system for controlling ignition. The ignition system gives a spark energy of ~1 mJ [6], which is more than the minimum ignition energy of the fuels tested in the present study. Gaseous fuel–air mixtures are prepared by using their partial pressures. For liquid fuel–air mixture preparation, a calibrated amount of liquid fuel is injected into a stainless steel chamber. Before the injection of liquid fuel, the stainless steel chamber, combustion vessel, heat exchanger, and piping are heated to a temperature above the saturation temperature of the liquid fuel. A high-temperature circulation pump is connected in series with the injection chamber, combustion vessel, and heat exchanger; this ensures homogeneous mixture preparation inside the vessel. Five minutes are allowed for the mixture to become homogeneous and then a further 5 min for it to become quiescent. This is consistent with the earlier studies [2,6], as longer times make no difference to the burning velocity.

The methanol was injected through a calibrated solenoid injector, and there were then two independent checks on the air–fuel ratio (AFR). The pressure and temperature in the vessel were measured before and after addition of the fuel (allowing at least 5 min after injection of the fuel for equilibrium to be attained). The pressure was measured with a piezo-resistive pressure transducer that had been calibrated against a mercury manometer, and the accuracy of determining the AFR with this method was considered to be better than 1%. After combustion a Lambda sensor was used to check the AFR. On average the AFR was within 0.5% of the target AFR, and (within the three-significant-figure resolution of the Lambda sensor) there was no difference between the AFR measured by the Lambda sensor and the value deduced from the partial pressure.

A Kistler 701A quartz pressure transducer was used with a Kistler 5001 charge amplifier for the measurement of the dynamic pressure. A high-speed data acquisition system based on a Pentium III PC with a National Instrument's Data acquisition (DAQ) card is set to record the pressure and ignition signal for the subsequent analysis. The DAQ system consists of a PCI-MIO-16E1 card, which provides 12 bits ana-

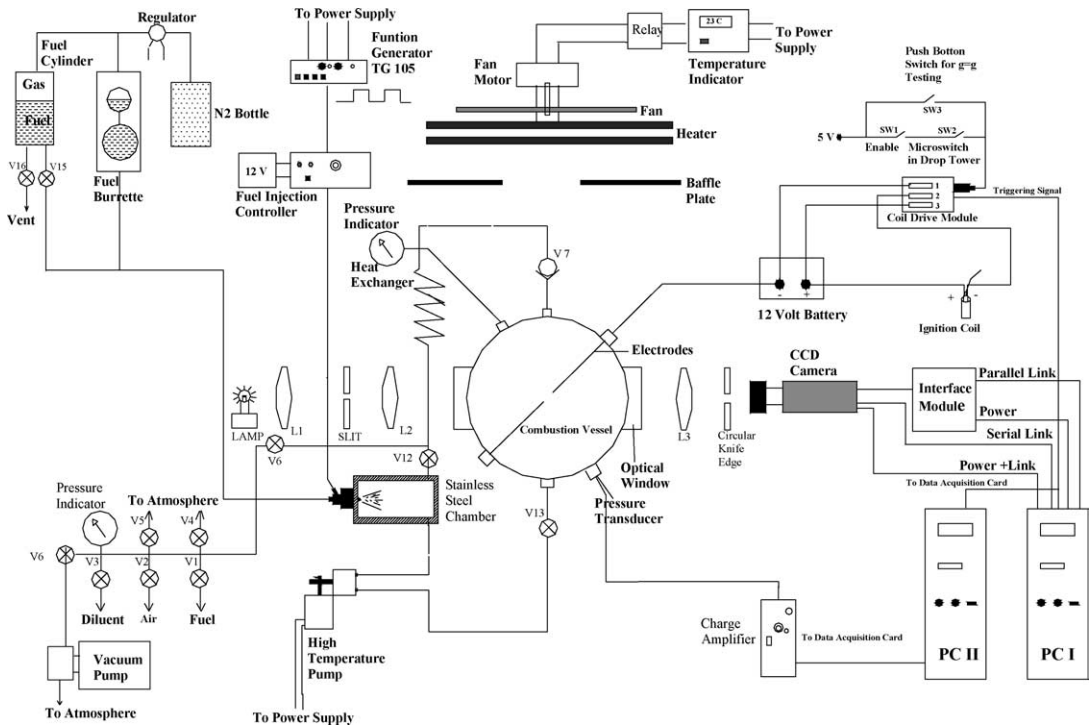


Fig. 6. Schematic representation of the experimental facility.

logue to digital conversion, a BNC-2090 rack mount, and the LABVIEW programming language for coding the data acquisition “front panel.” The data sampling rate was set at 25 kHz and the dynamic pressure measurement is triggered by the voltage history of the primary circuit of the ignition coil. The fuel injector was calibrated so as to determine the injection period for which the injector had to be opened for injecting the desired quantity of liquid fuel. The system arrangement and method of calibration is explained in [15].

Previous work [6] has shown that when the burning velocities are above 20 cm/s (as is the case here), the effect of buoyancy is less than 0.5% on the observed burning velocity. However, it is worth noting that, had we used our free-fall facility, in the comparatively few cases for which there was no cellularity, data over a slightly wider pressure range could have been analyzed [6]. In the current tests the optical access was not used, but earlier tests [18] in which the windows were replaced with concave-faced blanks to preserve the spherical surface showed no difference on the combustion process. The disturbance caused by the electrodes is another possible concern. These cannot be eliminated, but earlier tests [6] in which two additional dummy electrodes were added showed no affect on the pressure history.

## 5. Burning velocity calculation

The use of the multizone model for the determination of the laminar burning velocity is explained in Appendix A. A 10-zone equal mass model was selected, where the burned gas is divided into zones of equal mass. To determine the burning velocities and other properties of the fuel–air mixtures, a program (BURNVEL) takes the output files of the BOMB program and the data files from the experiments. Table 2 shows a comparison of the maximum pressure for the 10 equal mass zones BOMB program files with that of the single zone STANJAN [4] program. It can be seen

Table 2  
Comparison of maximum pressures from the BOMB and STANJAN program

$\phi$	$P_{\max}$ (BOMB)	$P_{\max}$ (STANJAN)	Difference (%)
0.7	7.50	7.555	0.76
0.8	8.03	8.089	0.70
0.9	8.48	8.53	0.51
1	8.82	8.85	0.32
1.1	8.99	9.02	0.37
1.2	9.03	9.07	0.45
1.3	9.02	9.01	−0.03
1.4	8.97	8.94	−0.30

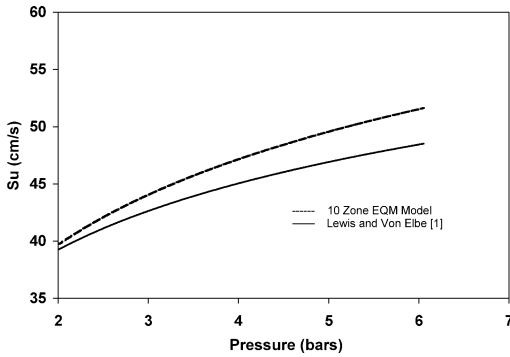


Fig. 7. Burning velocity ( $S_u$ ) as a function of pressure and temperature, as calculated from the 10-zone model and the Lewis and von Elbe method [1] for the combustion of a stoichiometric methanol–air mixture at 325 K and 1 bar initial conditions.

that the difference in the maximum pressure is mostly less than 0.5%, which is negligible. Systematic experimental measurements of the laminar burning velocity of methanol–air mixtures have been made for varying equivalence ratio (0.8–1.5, with 0.1 steps), initial temperature (either 293.15 or 425 K), and pressure (0.5, 1.0, 2.0, and 3.5 bar). However, with the bomb method, data are produced for much higher temperature and pressures.

## 6. Errors associated with the use of a single burned gas model

Stone et al. [3] reported that if the end pressure is calculated by means of the STANJAN [4] program then the Lewis and Von Elbe [1] method and the more rigorous single zone burned gas model of Metghalchi and Keck [2] gave very similar results. However, as shown in Fig. 7, in the present study it was found that the Lewis and von Elbe [1] method underpredicts the pressure by up to about 6%, and the error is a maximum for stoichiometric conditions. Fig. 8 shows the difference in the burning velocity calculated from the Lewis and von Elbe [1] method and that from the present 10-zone EQM models as a function of simultaneous rise of pressure and temperature for a typical test run. The percentage difference increases with the simultaneous increase of pressure and temperature.

During the initial stages of combustion, the flame front has high values of flame stretch due to the large curvature that is associated with a small spherical surface. However, in a spherical vessel the radius of curvature increases and the flame stretch approaches zero asymptotically, and the ideal case for a plane flame front is approached. Since there is negligible pressure rise associated with the initial flame propagation, these data are not used, and flame stretch effects can

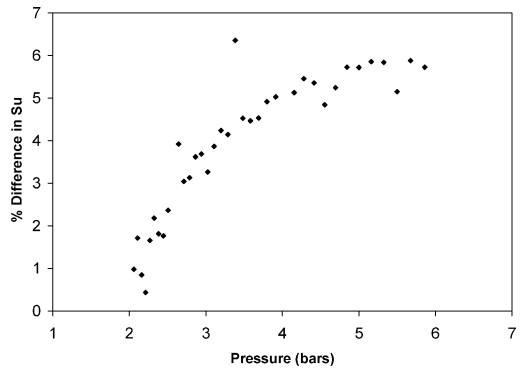


Fig. 8. Percentage difference in the burning velocity as calculated from the 10-zone model and Lewis and von Elbe method [1] for a stoichiometric methanol–air mixture at 325 K and 1 bar initial conditions.

be ignored; a fuller justification for this is provided by Stone et al. [3].

The laminar burning velocity data are obtained from many experiments and fitted with the same form of correlation as that used by Stone et al. [3] to show the dependency of the laminar burning velocity on pressure, temperature, and equivalence ratio:

$$S_u = [S_{u,0} + S_{u,1}(\phi - 1) + S_{u,2}(\phi - 1)^2 + S_{u,3}(\phi - 1)^3 + S_{u,4}(\phi - 1)^4][T^\alpha P^\beta], \quad (1)$$

where  $S_{u,0}$ ,  $S_{u,1}$ ,  $S_{u,2}$ ,  $S_{u,3}$ ,  $S_{u,4}$ ,  $\alpha_1$ ,  $\beta_1$ ,  $\alpha_0$ , and  $\beta_0$  are the coefficients,

$$T = T_u/T_0, \quad P = P_u/P_0,$$

$$\alpha = \alpha_0 + (\phi - 1)\alpha_1, \quad \text{and} \quad \beta = \beta_0 + (\phi - 1)\beta_1.$$

A least squares method [3] has been used for fitting the correlation to the experimental data.

## 7. Experimental results

Methanol has been studied since there is a shortage of laminar burning velocity data for methanol at elevated temperatures and pressures. In particular, the previous data available for methanol at elevated temperatures and pressures did not appear to take into consideration the formation of cellular flames, thereby making the reported correlation susceptible to large errors.

### 7.1. Burning velocity as a function of temperature and pressure

Fig. 9 shows the values for the laminar burning velocity along the unburned gas isentropes plotted against both temperature and pressure for the different equivalence ratios and specified initial temperature

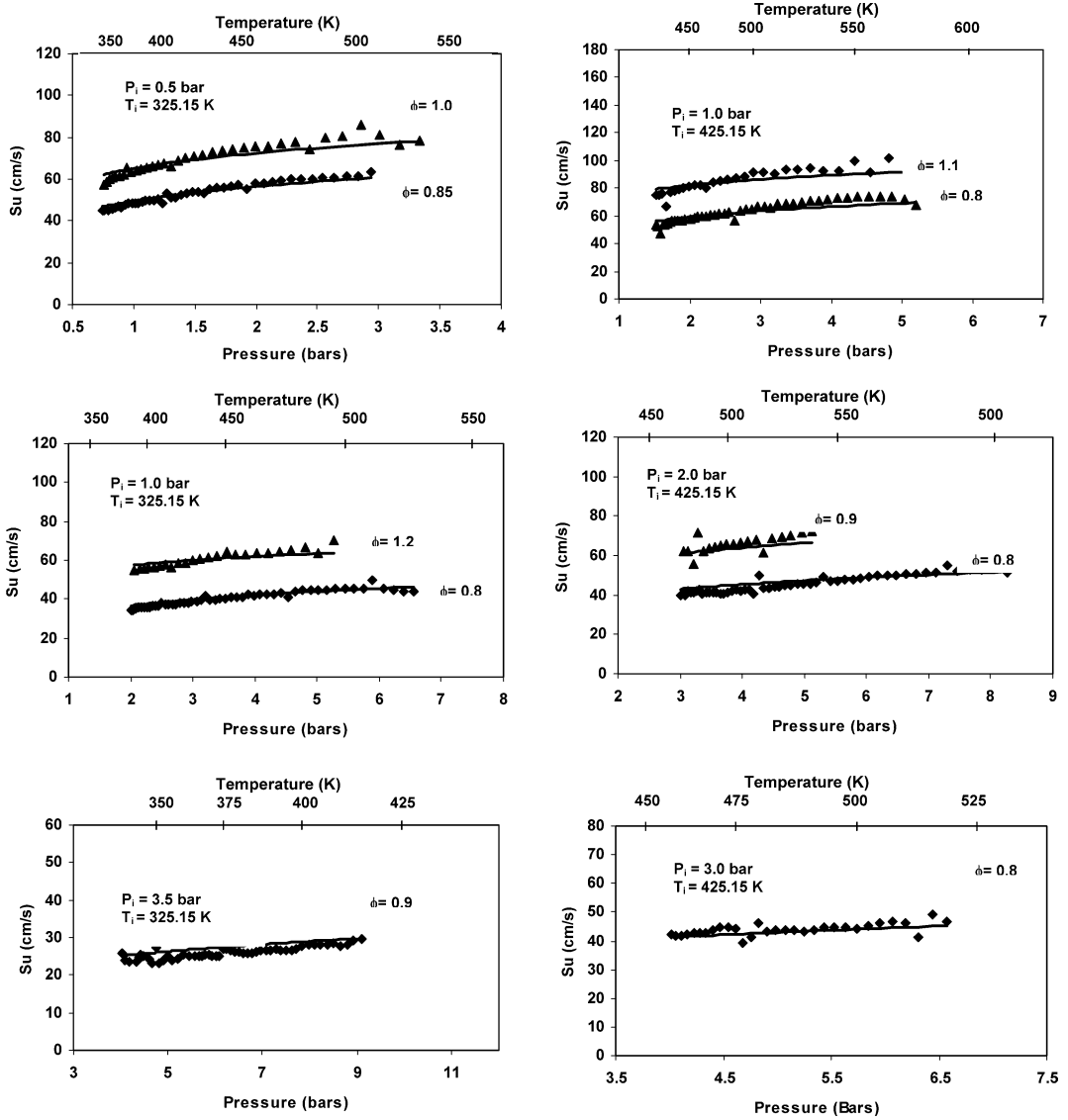


Fig. 9. The methanol/air burning velocity as a function of pressure and temperature, for different initial temperatures, pressures, and equivalence ratios, showing a comparison between the experimental data and the correlation.

Table 3  
Values of the coefficients obtained using the correlation in Eq. (1)

$S_{u,1}$	$S_{u,2}$	$S_{u,3}$	$S_{u,4}$	$\alpha_1$	$\beta_1$	$S_{u,0}$	$\alpha_0$	$\beta_0$
0.5894	-2.2727	-2.0137	6.9062	-1.317	0.1499	0.4614	1.3209	-0.1807

and pressures. Solid lines indicate the values obtained from the correlation. Table 3 gives the final values of the coefficients obtained and Table 4 gives the range of application of the correlation. It was found that the correlation gave a very good fit for most of the data. Fig. 9 shows that the correlation gives a good fit to the experimental data. The maximum deviation of the

correlation from the experimental data points is at the later stages of combustion. This may be due to the presence of asymmetry in the flame front (and hence quenching of some parts of the flame front at the vessel wall earlier than other parts) or the inclusion of a few data points from cellular flames. An attempt was made to use a second order correlation (as proposed

Table 4  
Range of validity for the correlation coefficients in Table 3

Initial Temp (K)	P (bar)	T (K)	$\phi$	$S_u$ (cm/s)
325–425	0.5–13.5	295–650	0.7–1.5	> 10

by Metghalchi and Keck [11]) to fit the current experimental data, but the residual error was found to be very large.

Fig. 9 also shows that data from the early flame growth was not used—the data selected are indicated by the range over which the correlation has been evaluated. Typically, the only data analyzed are those after the pressure has risen by about 50%, so as to be able to ignore the effects of stretch. The density ratio between the burned and the unburned gases is such that even this small pressure rise will be associated with a flame radius of above 5 cm and a strain rate of about  $0.01 \text{ s}^{-1}$  which will introduce an error of the order of 1% in the burning velocity. Previous work at Oxford has considered this issue in more detail [6]. As the flame develops, its radius increases and the flame speed reduces, so that the effects of strain reduce further. The nature of the data fitting, which employs data from a range of pressures in each run and from runs with different initial temperatures and pressures, will further reduce the effect of burning velocity measurements influenced by stretch.

### 7.2. Burning velocity as a function of the equivalence ratio

Fig. 10 shows the comparison of the burning velocities for methanol–air mixture at 298 K and 1 bar obtained from the present work with those of the most recently reported data of Davis and Law [19], who used a counterflow twin-flame technique. Also shown for comparison are the earlier data of Gülder [20] and Metghalchi and Keck [11] (both of whom used the constant-volume spherical vessel technique) and Gibbs and Calcote [21] (who used a burner technique). The large deviation between the Metghalchi and Keck [11] correlation and the experimental data in Fig. 10 may be due to the errors associated with the method applied by Metghalchi and Keck [11] for the determination of the burning velocity and the inclusion of cellular flame data points. Fig. 10 shows that the burning velocities obtained from the present study show very good agreement with the data of Davis and Law [19]. For all equivalence ratios, the differences in burning velocities obtained in the present study and in the data of Davis and Law [19] are very low and the greatest difference is around 8% at  $\phi = 0.9$ . This may be attributed to the presence of errors associated with strain corrections in the twin flame technique as

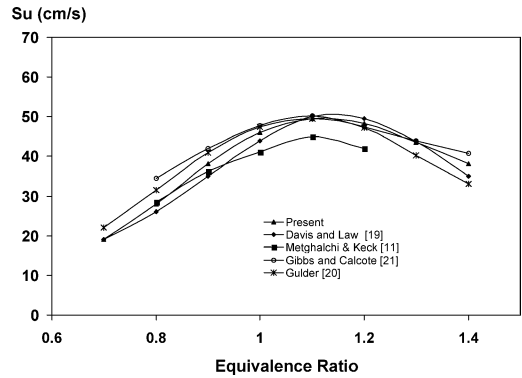


Fig. 10. Comparison of the methanol/air burning velocity ( $S_u$ ) at 298 K and 1 bar with earlier reported data.

discussed above. The maximum burning velocity obtained from the present study is  $49.6 \text{ cm/s}$  at  $\phi = 1.10$  and at the same equivalence ratio Davis and Law [19] reported a burning velocity of  $50 \text{ cm/s}$ . It can be seen from Fig. 9 that the data reported by Metghalchi and Keck [11] give good agreement with the present data at equivalence ratios of 0.8 and 0.9. However, their study gives lower burning velocities for equivalence ratios richer than 0.9. Gülder [20] reported a maximum burning velocity of  $49.2 \text{ cm/s}$  at  $\phi = 1.1$ . This is in agreement with the data obtained in the present study and with the work of Davis and Law [19]. However, Gülder [20] reported higher burning velocities on the lean side and lower on the rich side, compared with the present work and that of Davis and Law [19]. Metghalchi and Keck [11] and Gülder [20] both used a closed spherical vessel for their burning velocity measurements, but neither of these studies indicated the formation of cellular flames inside the vessel. The higher burning velocities reported by Gülder [20] may be due to the use of data having cellular flames and the large errors associated with the use of an exponential form of correlation for fitting the data; it appears that the coefficients for the exponential term vary erratically with equivalence ratio. The data reported by Metghalchi and Keck [11] for methanol–air mixtures also indicate the formation of cellular flames, but their correlation includes these data and has errors associated with using a single-burned-zone model. Gibbs and Calcote's [21] data are in substantial disagreement with the present study; this is likely to be due to the errors associated with no stretch compensation and to experimental errors such as the correct measurement of the flame area and a large heat loss to the burner wall (thereby reducing the flame velocity at the walls).

The errors associated with deducing the AFR have been quantified as below 0.5%. The errors associated with recording the pressure data are easy to quantify, but the errors associated with pressure analysis

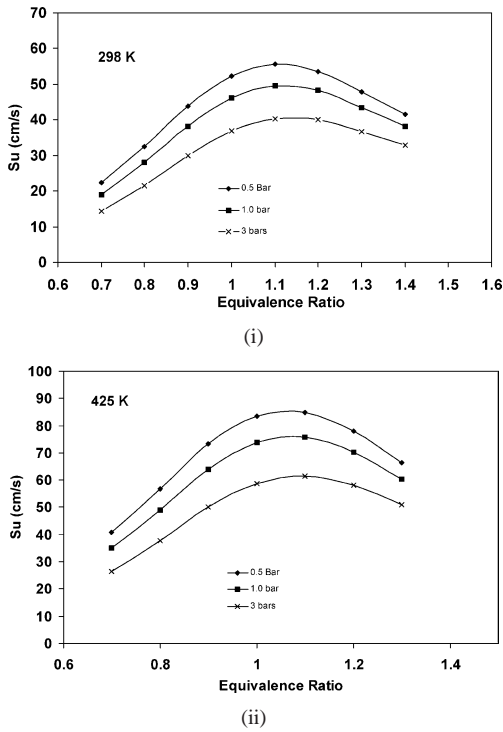


Fig. 11. Burning velocity ( $S_u$ ) as a function of equivalence ratio for varying initial pressures of 0.5, 1, and 3.0 bar and fixed temperatures of (i) 298 K and (ii) 425 K.

are much more difficult to quantify. The piezo-electric transducer and its amplifier were calibrated regularly over different pressure ranges with a dead-weight tester. The long-term repeatability of the calibration was better than 1% for the three pressure ranges used. A sensitivity study showed that a 1% error in the pressure transducer calibration would lead to a 0.25% error in the burning velocity. Furthermore, the least squares fitting of the analytical function to describe the burning velocity will have the effect of reducing the significance of errors on the individual measurements, albeit in a way that is very difficult to quantify. However, the quality of the correlation fit to the experimental data (Fig. 9) and the close agreement with the data of Davis and Law [19] (Fig. 10), which is mostly within 1 cm/s, both provide reassurance about the accuracy of the correlation.

### 7.3. Burning velocity as a function of pressure

Fig. 11 shows the variation of burning velocity as a function of equivalence ratio and pressure at two fixed temperatures. It can be seen from Fig. 11 that the burning velocity decreases with the increase in pressure. The values of the burning velocities at a fixed unburned gas temperature but varying pressure are obtained directly from the BURNVEL program.

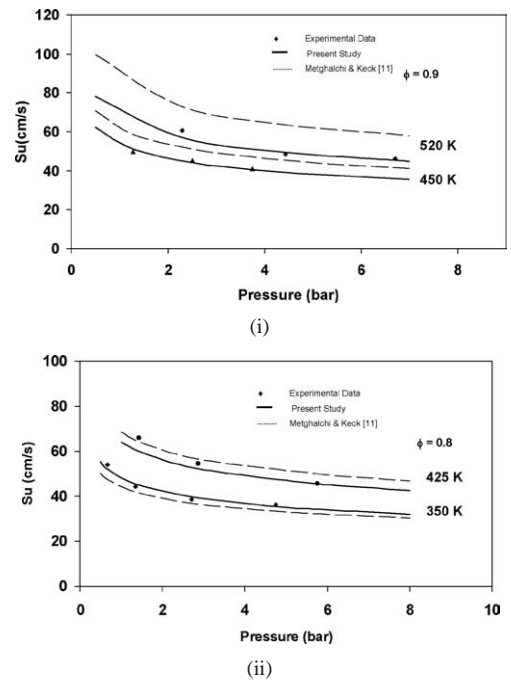


Fig. 12. Effect of the pressure on the burning velocity ( $S_u$ ). Solid lines indicate the correlation fit. (i) Equivalence ratio of 0.9 and an initial temperature of 323.15 K; (ii) equivalence ratio of 0.8 and an initial temperature of 425 K.

Fig. 12 shows the variation of the burning velocity as a function of pressure for the different temperatures and equivalence ratios. It can be seen from Fig. 12 that the burning velocity decreases with an increase in pressure. The fourth order correlation fitted to the experimental data gives a very good fit for the different fixed unburned gas temperature data. The Metghalchi and Keck [11] second order correlation has also been plotted for comparison. Fig. 12 shows that for a fixed unburned gas temperature of 350 K, the Metghalchi and Keck [11] correlation gives higher burning velocities than the correlation from the present study. However, for higher fixed unburned gas temperature conditions, it overpredicts the burning velocity. This may be attributed to their inadvertent use of data from cellular flames. Comparisons could not be made with the correlations of Ryan and Lestz [10] and Gülder [20] as they provided values of the coefficients only for stoichiometric mixtures. In the present study, a comparison for stoichiometric conditions is not possible because, at higher pressure conditions, cellularity was found to trigger at a very early stage.

### 7.4. Burning velocity as a function of temperature

Fig. 13 shows the variation of the burning velocities as a function of unburned gas temperature with fixed pressure. Fig. 13i (from test runs having differ-

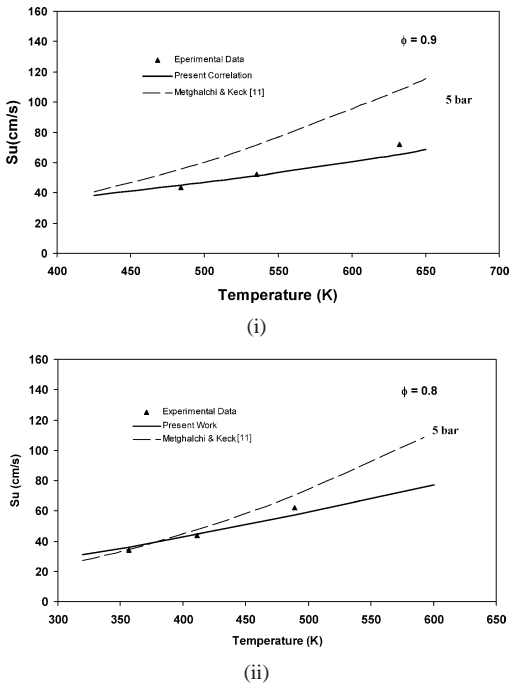


Fig. 13. Effect of the temperature on the burning velocity at a pressure of 5 bar. (i) Equivalence ratio of 0.9; (ii) equivalence ratio of 0.8; from test runs having different initial temperatures and pressures.

ent initial temperatures and pressures) has an equivalence ratio of 0.9 and a fixed pressure of 5 bar. Similarly, Fig. 13ii is for an equivalence ratio 0.8 and a fixed pressure of 5 bar. It can be seen from Fig. 13 that at a fixed pressure the burning velocities for methanol increase with temperature. The fourth order correlation gives a good fit to the experimental data for both equivalence ratios, but the burning velocities given by the Metghalchi and Keck [11] correlation increase considerably faster than was observed in the present study.

In the spherical vessel, the unburned gas temperature and pressure are coupled, but the temperature effect dominates over the pressure effect for most fuels, and this leads to the increase in burning velocities with the simultaneous increase in temperature and pressure.

### 7.5. Cellular flames

Investigators such as Gülder [20], Metghalchi and Keck [11], and Ryan and Lestz [10] who used the constant-volume method for the determination of the burning velocities have assumed that the flame front is smooth, with no cellularity or wrinkling of the flames. However, cellular flames can be formed under certain conditions, and in the present study cellularity was

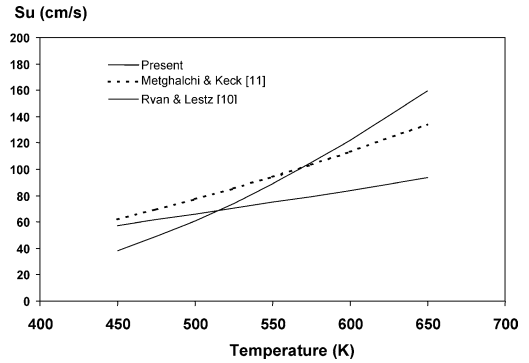


Fig. 14. Comparison of the burning velocities of stoichiometric methanol-air mixtures as a function of unburned gas temperature, as correlated by Ryan and Lestz [10], Metghalchi and Keck [11], and in this study at 6 bar.

found to exist for methanol-air flames. When cellularity triggers, the increase in the surface area leads to a sudden increase in the burning velocity and any inclusion of these data points would lead to higher burning velocity predictions. Metghalchi and Keck [11] did not mention the cellular flames in their study and their higher burning velocities could be attributed to the inclusion of the cellular flame data. Burning velocities derived from Metghalchi and Keck [11] are found to increase at a much faster rate for the initial temperature of 425 K than for 323 K. Ryan and Lestz [10] also measured the burning velocities in spherical vessels. Fig. 14 gives a comparison of the values obtained from the correlations from the present study, Metghalchi and Keck [11], and Ryan and Lestz [10] for a stoichiometric mixture at 6 bar.

It can be seen from Fig. 15 that the burning velocities from Ryan and Lestz [10] give lower burning velocities than the present study at temperatures lower than 520 K. The reason for this could be due to the inclusion of cellular flame data, the methodology used in the determination of burning velocities, or the sensitivity of the exponential correlation to temperature. Fig. 15 shows the onset of cellularity in test runs with initial conditions of 1 bar, 323 K, and different equivalence ratios; vertical lines indicate the onset of cellularity. It can be seen from the figures that the cellularity leads to an increase in the values of the burning velocities. This is due to the transformation of the smooth spherical flame front to the polyhedral flame structures which increase the surface area of the flame front, thereby invalidating the smooth flame assumption. No cellular flames were found to exist with initial conditions of 0.5 bar, at either 323 or 425 K for any range of fuel-air equivalence ratios. However, cellularity was found to occur in test runs with initial conditions of 1, 2, 3, or 3.5 bar and initial temperatures of 323 and 425 K. Table 5

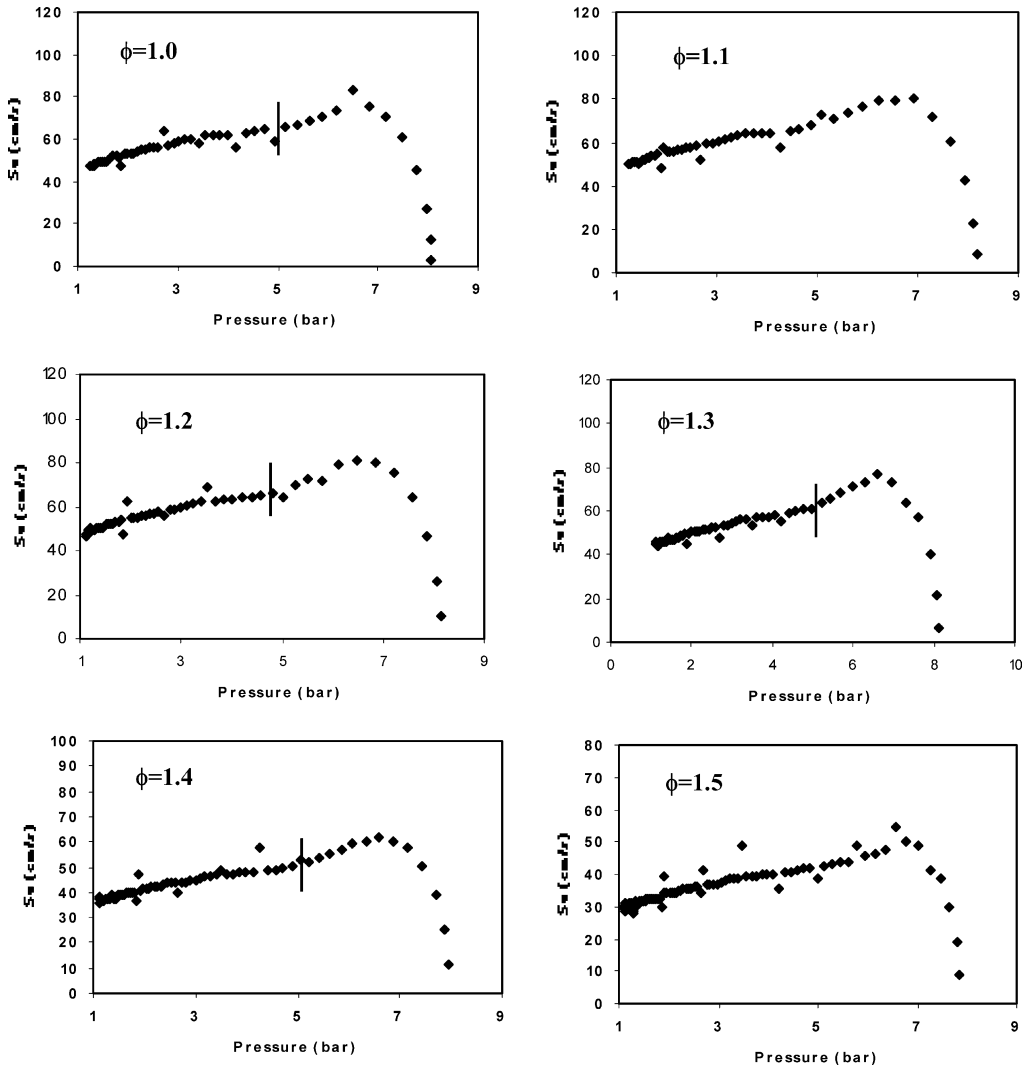


Fig. 15. Formation of cellular flames in the spherical vessel, for methanol–air mixtures with initial conditions of 323 K and 1 bar.

shows the critical time, pressure, and equivalence ratios at which cellularity was found to trigger for the methanol–air mixtures. In the present study, cellular flame data points were excluded from the burning velocity correlation.

## 8. Conclusions

A novel multizone model has been used to study the combustion process inside a closed vessel. Findings include the following.

- (1) A 10-zone model with 200 steps gives sufficiently accurate results to describe combustion inside a spherical vessel.
- (2) A temperature difference exists between the first and the last burned gas zones. For methane/air fuel mixtures this difference is as large as 500 K.
- (3) The relationship between the pressure rise and the mass fraction burned is nonlinear. The errors associated with the linear assumption peak at 0.1–0.2 mass fraction burned for all the equivalence ratios tested. The maximum error was found to be for stoichiometric mixtures.
- (4) The burned gas temperature profile has an effect on the end pressure for methane and the error when ignoring it can be as large as 5%.
- (5) The multizone burning velocity technique has been successfully used for the determination of the laminar burning velocities of methanol–air mixtures at varying equivalence ratios, temperatures, and pressures.

Table 5

Temperature, pressure, and time for the formation of cellular flames

$T_i$ (K)	$P_i$ (bars)	$\phi$	$t_c$ (ms)	$T_c$ (K)	$P_c$ (bars)
323	1.0	1.0	34.4	508.1	5.89
323	1.0	1.1	31.2	488.6	5.09
323	1.0	1.2	30.8	480.3	4.80
323	1.0	1.3	34.0	483.7	4.98
323	1.0	1.4	42.0	487.8	5.23
323	1.0	1.5	51.2	495.9	5.60
323	2.0	0.85	42.8	435.1	6.21
323	2.0	0.9	36.4	432.2	6.10
323	2.0	1.0	28.8	411.6	5.07
323	3.5	0.8	60.0	425.2	9.95
323	3.5	0.9	24.4	360.4	5.29
425	1.0	1.5	28.4	602.2	4.51
425	2.0	0.8	56.4	609.3	8.46
425	2.0	0.9	28	538.0	5.12
425	3.0	0.8	41.6	521.2	6.70
425	3.0	0.9	23.2	483.6	5.00

- (6) The burning velocity for methanol–air mixture has been compared with the earlier reported data of Davis and Law [19], Gülder [20], Metghalchi and Keck [11], and Gibbs and Calcote [21]. The values obtained from the present study give very good agreement with the recently reported data of Davis and Law [19]. Comparisons with the correlation proposed by Metghalchi and Keck [11] for the varying pressure and temperature show that Metghalchi and Keck overpredict the burning velocities for a range of varying pressure and temperatures.
- (7) Cellular flames have been found to exist in the test runs reported here, and Table 5 summarizes the conditions at their formation with regard to the initial unburned gas temperature, initial pressure, equivalence ratio, and the time, pressure, and temperature at its onset.

## Appendix A. Multizone model

$c_p$	Specific heat
$e$	Specific internal energy
$E$	Internal energy
$h$	Specific enthalpy
$m$	Mass
$p$	Pressure
$S$	Entropy
$S_u$	Burning velocity
$T$	Temperature
$v$	Specific volume
$V$	Volume
$x$	Mass fraction burned

## Subscripts

$b$	Burned
$0, i$	Initial condition
$u$	Unburned condition
$w$	Wall

The burning velocity calculations are based on using a spherical closed vessel filled with homogeneous combustible mixture. At time  $t = 0$ , the mixture is ignited at the center; a spherical flame front is established instantaneously and begins to propagate outwardly to reach the wall. The following assumptions are used in the analysis of the behavior of the system during this interval.

- (i) Prior to the onset of ignition, the unburned gas is initially at rest and the gas has a uniform temperature and composition.
- (ii) The thickness of the reaction zone is negligible, and the flame front is smooth and spherical.
- (iii) The burnt gas fraction  $x$  is at local thermodynamic and chemical equilibrium.
- (iv) The unburned gas fraction  $(1 - x)$  is at local equilibrium but with fixed (original) chemical composition.
- (v) The pressure within the combustion vessel is a function of time only and is independent of the flame front.
- (vi) The compression path of both the unburned and the burned gas is adiabatic and reversible.
- (vii) The gas behaves as a semiperfect gas.
- (viii) The effects of body forces and of radiative energy transfer can be neglected.
- (ix) There is no heat transfer between the burned and the unburned gases.

With these assumptions, the burning velocity equation is derived using the multizone model in the following way.

Consider an elemental shell of thickness  $dr_i$  at radius  $r_i$ . If, during the travel of the flame through the vessel, the burned gas had not expanded, then an element  $dr_i$  would be the thickness of a shell at the temperature  $T_i$  and pressure  $P_i$  about to be traversed by the wave in the time element  $dt$ , as shown in Fig. 16a. Its volume would have been:

$$4\pi r_i^2 dr_i. \quad (\text{A.1})$$

However, by expansion, the radius of the shell increased from  $r_i$  to  $r_b$ , the pressure increased to  $P$ , and the temperature of the shell increased to  $T_u$ . Therefore, its volume is actually

$$4\pi r_i^2 dr_i \left( \frac{T_u P_i}{T_i P} \right). \quad (\text{A.2})$$

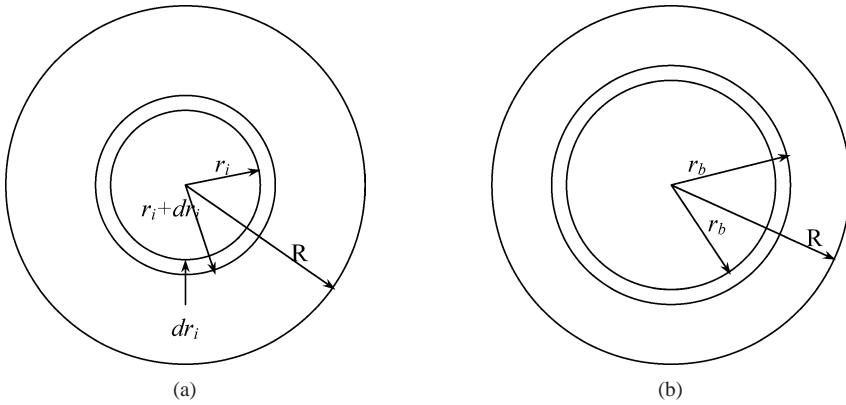


Fig. 16. Position of the elemental shell (a) before burning and (b) after burning.

Since the thickness of the shell is equal to  $S_u dt$ , its volume is also equal to

$$4\pi r_b^2 S_u dt. \tag{A.3}$$

By equating Eqs. (A.2) and (A.3) one obtains the equation for the burning velocity as

$$S_u = \left(\frac{dr_i}{dt}\right) \left(\frac{r_i}{r_b}\right)^2 \left(\frac{T_u P_i}{T_i P}\right). \tag{A.4}$$

However, the unburned gas is assumed to be undergoing isentropic compression, so the unburned gas temperature can be calculated by

$$T_u = T_i \left(\frac{P}{P_i}\right)^{(\gamma_u - 1)/\gamma_u}. \tag{A.5}$$

Substituting Eq. (A.5) into Eq. (A.4) gives the equation for burning velocity as

$$S_u = \left(\frac{dr_i}{dt}\right) \left(\frac{r_i}{r_b}\right)^2 \left(\frac{P_i}{P}\right)^{1/\gamma_u}. \tag{A.6}$$

This is the equation derived by Lewis and von Elbe [1], who also assumed that the fractional pressure rise was proportional to the mass fraction burned. However, Lewis and von Elbe do not include the temperature gradient established in the burned gas region and the changes in the burned gas properties and compositions due to it. The above assumptions can be avoided by using a mathematical derivation of the time-dependent first order ordinary differential equations for the pressure and burned and unburned gas temperatures. The derivation is done by first dividing the mixture into single burned and unburned zones separated by a flame front of zero thickness. The single burned zone is then extended to multiple zones, which enables the incorporation of the burned gas temperature gradient in the model. For a constant-volume vessel a differential form of the energy conservation equation is given as

$$m \frac{de}{dt} - \frac{dQ}{dt} = 0. \tag{A.7}$$

At any instant during combustion, the contents of the closed vessel consist of the burned and the unburned gases separated by the flame front of zero thickness. The equations for the conservation of volume and internal energy are given by Eqs. (A.8) and (A.9):

$$v = \frac{V}{M} = xv_b(P, T_b) + (1-x)v_u(P, S_u, 0), \tag{A.8}$$

$$e = \frac{E}{M} = xe_b(P, T_b) + (1-x)e_u(P, S_u, 0). \tag{A.9}$$

Based on the work of Ferguson [16], the above three equations are solved as a set of the ordinary differential equations for the rate of change of pressure and burned and unburned gas temperatures for a single burned zone. These differential equations are then extended to the multiple burned gas zones for the multizone analysis. The differential equations for the pressure and unburned and burned gas temperatures are given by the equations

$$\frac{dP}{dt} = \frac{B}{C + D}, \tag{A.10}$$

$$\frac{dT_u}{dt} = \frac{v_u}{C_{pu}} \frac{\partial \ln v_u}{\partial \ln T} \left(\frac{B}{C + D}\right), \tag{A.11}$$

and

$$\begin{aligned} \frac{dT_b}{dt} = & -(1-x) \frac{v_u}{T_u} \frac{\partial \ln v_u}{\partial \ln T_u} \frac{T_b}{xv_b} \frac{\partial \ln T_b}{\partial \ln v_b} \\ & \times \frac{v_u}{C_{pu}} \frac{\partial \ln v_u}{\partial \ln T_u} \frac{\partial \ln v_u}{\partial \ln T_u} \left(\frac{B}{C + D}\right) \\ & - \frac{T_b}{xv_b} \frac{\partial \ln T_b}{\partial \ln v_b} \left(x \frac{v_b}{P} \frac{\partial \ln v_b}{\partial \ln P}\right) \\ & + (1-x) \frac{v_u}{P} \frac{\partial \ln v_u}{\partial \ln P} \left(\frac{B}{C + D}\right) \\ & - \frac{T_b}{xv_b} \frac{\partial \ln T_b}{\partial \ln v_b} (v_b - v_u) \frac{dx}{dt}, \end{aligned} \tag{A.12}$$

where

$$B = \left( (v_u - v_b) + \frac{v_b}{C_{p,b} T_b} (h_b - h_u) \right) \frac{dx}{dt}, \tag{A.13}$$

$$C = x \left( \frac{v_b^2}{C_{pb} T_b} \left( \frac{\partial \ln v_b}{\partial \ln T_b} \right)^2 + \frac{v_b}{P} \frac{\partial \ln v_b}{\partial \ln P} \right), \quad (\text{A.14})$$

and

$$D = (1-x) \left( \frac{v_u^2}{C_{pu} T_u} \left( \frac{\partial \ln v_u}{\partial \ln T_u} \right)^2 + \frac{v_u}{P} \frac{\partial \ln v_u}{\partial \ln P} \right). \quad (\text{A.15})$$

For the multizone analysis, the above equations are extended to  $N$  zones. Now,  $N + 3$  equations need to be solved simultaneously. The extension of the single burned gas zone to multiple zones is done as

$$\frac{dP}{dt} = \frac{B_u + \sum B_i}{\sum C_i + D}, \quad (\text{A.16})$$

$$\frac{dT_u}{dt} = \frac{v_u}{C_{pu}} \frac{\partial \ln v_u}{\partial \ln T} \left( \frac{B_u + \sum B_i}{\sum C_i + D} \right), \quad (\text{A.17})$$

and

$$\begin{aligned} \frac{dT_{bi}}{dt} = & -(1-x) \frac{v_u}{T_u} \frac{\partial \ln v_u}{\partial \ln T_u} \frac{T_{bi}}{x v_{bi}} \frac{\partial \ln T_{bi}}{\partial \ln v_{bi}} \\ & \times \frac{v_u}{C_{pu}} \frac{\partial \ln v_u}{\partial \ln T_u} \frac{\partial \ln v_u}{\partial \ln T_u} \left( \frac{B_u + \sum B_i}{\sum C_i + D} \right) \\ & - \frac{T_{bi}}{x v_{bi}} \frac{\partial \ln T_{bi}}{\partial \ln v_{bi}} \left( x \frac{v_{bi}}{P} \frac{\partial \ln v_{bi}}{\partial \ln P} \right. \\ & \left. + (1-x) \frac{v_u}{P} \frac{\partial \ln v_u}{\partial \ln P} \right) \left( \frac{B_u + \sum B_i}{\sum C_i + D} \right) \\ & - \frac{T_{bi}}{x v_{bi}} \frac{\partial \ln T_{bi}}{\partial \ln v_{bi}} (v_{bi} - v_u) \frac{dx}{dt}, \quad (\text{A.18}) \end{aligned}$$

where  $\sum(B_i) = B_1 + B_2 + B_3 + \dots + B_n$ ,

$$B_u = (v_u - h_u) \frac{dx}{dt}, \quad (\text{A.19})$$

$$B_i = \left( -v_{bi} + \frac{v_{bi}}{C_{p,bi} T_{bi}} h_{bi} \right) \frac{dx}{dt}, \quad (\text{A.20})$$

$$C_i = x \left( \frac{v_{bi}^2}{C_{pbi} T_{bi}} \left( \frac{\partial \ln v_{bi}}{\partial \ln T_{bi}} \right)^2 + \frac{v_{bi}}{P} \frac{\partial \ln v_{bi}}{\partial \ln P} \right), \quad (\text{A.21})$$

and

$$D = (1-x) \left( \frac{v_u^2}{C_{pu} T_u} \left( \frac{\partial \ln v_u}{\partial \ln T_u} \right)^2 + \frac{v_u}{P} \frac{\partial \ln v_u}{\partial \ln P} \right). \quad (\text{A.22})$$

Burned gas volume and radius are calculated from the following equations:

$$v_b = V - m_i(n-1)(RuT_u/P) \quad (\text{A.23})$$

and

$$r_b = R(V - m_i(n-1)(RuT_u/P)). \quad (\text{A.24})$$

The burning velocity in the present method is then calculated by utilizing this multizone model. This is

done by modifying Eq. (A.6) to

$$S_u = \left( \frac{dp}{dt} \right) \left( \frac{dr_i}{dp} \right) \left( \frac{r_i}{r_b} \right)^2 \left( \frac{P_i}{P} \right)^{1/\gamma_u}. \quad (\text{A.25})$$

In Eq. (A.25) the first term on the right hand side,  $dp/dt$ , is calculated from the experimental data file. The second term,  $dr_i/dp$ , is calculated from the BOMB program.

Since  $r_i$  and  $r_b$  are both functions of pressure,

$$r_i = f(p), \quad (\text{A.26})$$

$$r_b = f(p), \quad (\text{A.27})$$

$$x = \left( \frac{r_i}{R} \right)^3, \quad (\text{A.28})$$

and

$$r_i = \sqrt[3]{x} R. \quad (\text{A.29})$$

## References

- [1] B. Lewis, G. von Elbe, *J. Chem. Phys.* 2 (1934) 283–290.
- [2] M. Metghalchi, J.C. Keck, *Combust. Flame* 38 (1980) 143–154.
- [3] R. Stone, A. Clarke, P. Beckwith, *Combust. Flame* 114 (1998) 546–555.
- [4] STANJAN, Stanford University, 1987.
- [5] F. Rahim, M. Elia, M. Uliniski, M. Metghalchi, *Int. J. Eng. Res.* 3 (2) (2002) 81–92.
- [6] A. Clarke, Ph.D. thesis, Oxford University, 1994.
- [7] B. Hopkinson, *Proc. R. Soc. London A* 77 (1906) 387.
- [8] K.H. O'Donovan, C.J. Rallis, *Combust. Flame* 3 (1959) 201–214.
- [9] D. Bradley, A. Mitcheson, *Combust. Flame* 26 (1976) 201–217.
- [10] T.W. Ryan, S.S. Lestz, SAE Paper 800103, Detroit, 1980.
- [11] M. Metghalchi, J.C. Keck, *Combust. Flame* 48 (1982) 191–210.
- [12] P.G. Hill, J. Hung, *Combust. Sci. Technol.* 60 (1988) 7–30.
- [13] A. Spencer, R. Stone, E.P. Lim, S. Simonini, *J. Inst. Energy* 72 (1999) 157–164.
- [14] T. Takeno, T. Iijima, in: 7th International Colloquium on Gas Dynamics of Explosions and Reactive System, Gottingen, 1979, pp. 20–24.
- [15] K. Saeed, Ph.D. thesis, Oxford University, 2003.
- [16] G.R. Ferguson, *Internal Combustion Engines*, Wiley, New York, 1985.
- [17] S. Gordon, B. McBride, NASA SP-273, 1971.
- [18] C. Robinson, in: Joint Meeting of German and British Sections of the Combustion Institute, Cambridge, ISBN 0-9520350-0-6, March 1993.
- [19] S.G. Davis, C.K. Law, *Combust. Sci. Technol.* 140 (1998) 427–449.
- [20] O.L. Gülder, SAE Paper 841000, Detroit, 1984.
- [21] G.J. Gibbs, H.F. Calcote, *J. Chem. Eng. Data* 4 (1959) 226–237.